Vibrational spectra and thermal rectification in three-dimensional anharmonic lattices

Jinghua Lan

Department of Physics and Centre for Computational Science and Engineering, National University of Singapore,
Singapore 117542, Republic of Singapore

Baowen Li*

Department of Physics and Centre for Computational Science and Engineering, National University of Singapore,
Singapore 117542, Republic of Singapore
and NUS Graduate School for Integrative Sciences and Engineering,
Singapore 117597, Republic of Singapore

We study thermal rectification in a three-dimensional model consisting of two segments of anharmonic lattices. One segment consists of layers of harmonic oscillator arrays coupled to a substrate potential, which is a three-dimensional Frenkel-Kontorova model, and the other segment is a three-dimensional Fermi-Pasta-Ulam model. We study the vibrational bands of the two lattices analytically and numerically, and find that, by choosing the system parameters properly, the rectification can be as high as a few thousands, which is high enough to be observed in experiment. Possible experiments in nanostructures are discussed.

PACS number(s): 67.40.Pm, 63.20.Ry, 66.70.+f, 44.10.+i

I. INTRODUCTION

A thermal rectifier or thermal diode is a device that has a high or infinite thermal resistance in one direction whereas it has a low resistance when the temperature gradient is reversed. In the past several decades, there have been several experimental attempts to design such a thermal device.[1–4] However, a possible theoretical explanation of thermal rectification from the microscopic point of view became available only recently.[5] Terraneo *et al.*[5] introduced a one-dimensional (1D) model consisting of three segments of anharmonic (nonlinear) lattices with on-site Morse potential. By adjusting the nonlinear parameters appropriately, one can achieve a rectification between 1 and 2. The rectification is too low to be observed experimentally. Later on, a complete new model, a two-segment model was proposed by Li *et al.*[6] The two-segment model consists of two dissimilar anharmonic lattices, namely, the Frenkel-Kontorova (FK) lattice with different parameters in different parts. The nonlinearity of the lattice comes from the substrate interaction, the so-called on-site potential. By adjusting the parameters in the two segments, one can achieve a rectification as high as 200, which is two orders of magnitude better than that achieved with the three-segment model.

Furthermore, we find that the rectification, or asymmetric heat flow, results from an asymmetric thermal interface resistance—the Kapitza resistance.[7] By replacing one segment with a Fermi-Pasta-Ulam (FPU) lattice, the rectification can be improved to 2000, namely, one order of magnitude better than that achieved with the two-segment FK model.

Since a nonlinear lattice has many parameters to adjust, there are different possibilities to achieve the rectification, such as a change of potential periodicity.[8]

Most recently, we have extended the study of the thermal rectifier from a 1D to a two-dimensional (2D) lattice.[9] The rectification of the 2D model can be as much as several hundreds.

The aforementioned studies on 1D (Refs. 6–8) and 2D (Ref. 9) nonlinear lattices tell us that the determinant factor

for a thermal rectifier is the match and/or mismatch of the vibrational bands from the two segments. To this end, we need to (1) break the spatial symmetry of the system; (2) introduce nonlinearity (or anharmonicity). The broken spatial symmetry is necessary to make the heat flow asymmetric, while the introduction of the nonlinearity allows us to adjust the parameters to get match or mismatch of the vibrational spectra by reversing the temperature gradient. We know that the phonon band of a harmonic system will not change with temperature. Therefore, anharmonicity (nonlinearity) is essential to make the spectra temperature dependent.

In this paper, we make a step further, namely, we extend our study to a three-dimensional (3D) model. The extension is based on two reasons: (1) a three-dimensional or bulk material is closer to practical applications, and (2) extension to higher dimensions is scientifically more challenging, and of course more interesting.

The paper is organized as follows. In Sec. II, we describe our theoretical model and the numerical method used for computer simulation. In Sec. III, we provide theoretical analyses of spectra for two representative nonlinear lattices, the FK and FPU lattices, and make comparison with numerical results. Section IV is devoted to the numerical vibrational band of the two models under different parameters and prediction of suitable parameter settings for an efficient thermal rectifier. In Sec. V, we confirm our theoretical prediction by numerical evidence of strong rectification in our model. We end the paper with conclusions and discussion in Sec. VI.

II. MODEL AND METHODOLOGY

Like the 1D and 2D rectifier models, our 3D model also consists of two anharmonic lattices. One is a 3D FK lattice and another is a 3D FPU lattice. In the 3D FK lattice, we allow layered particles to move in the direction orthogonal to the substrate,[10] denoted as the *Z* direction. The description of anharmonic decay of a layered potential along the *Z* direction

must satisfy the following conditions: (a) as we get further away from the minimum, it should be harder to squeeze particles together than to separate them; and (b) asymptotic freedom: the particles should be free when their distance is large. We chose the Lennard-Jones potential form in the vertical Z direction,

$$V_s = \frac{A_0}{(2\pi)^2}\left[\left(\frac{z_{eq}}{z}\right)^{12} - \left(\frac{z_{eq}}{z}\right)^6 [\cos(2\pi x)\cos(2\pi y) + 1]\right].$$ (1)

z_{eq} is the equilibrium position along the Z direction. In this way, the 3D substrate potential reduces to the previous 2D sinusoidal form when $z=z_{eq}$. The +1 term after the cosine function makes the average potential zero at the plane $z=z_{eq}$. When $z<z_{eq}$ the average value is positive, and it is negative when $z>z_{eq}$. The potential barrier will decrease very fast along the Z direction.

The two parts are both simple cubic lattices with lattice constant a. The particle at the lth column in the X direction, the mth column in the Y direction, and the nth column in the Z direction is denoted as (l,m,n). The coordinates and momenta of this particle are $\vec{q}_{l,m,n}=(x_{l,m,n}, y_{l,m,n}, z_{l,m,n})$ and $\vec{p}_{l,m,n}=(p_{x_{l,m,n}}, p_{y_{l,m,n}}, p_{z_{l,m,n}})$. The Hamiltonian of a 3D array of harmonic oscillators and the 3D FPU lattice has the following form:

$$H = \sum_{l=1}^{N_X}\sum_{m=1}^{N_Y}\sum_{n=1}^{N_Z}\left(\frac{\vec{p}_{l,m,n}^2}{2} + kV(|\vec{r}_{l+1,m,n;l,m,n}| - a)\right.$$
$$\left. + kV(|\vec{r}_{l,m+1,n;l,m,n}| - a) + kV(|\vec{r}_{l,m,n+1;l,m,n}| - a)\right),$$ (2)

where $\vec{r}_{l_1,m_1,n_1;l_2,m_2,n_2}=\vec{q}_{l_1,m_1,n_1} - \vec{q}_{l_2,m_2,n_2}$ is the relative displacement between particles (l_1,m_1,n_1) and (l_2,m_2,n_2). N_X, N_Y, and N_Z are the number of particles along the X, Y, and Z directions, respectively. So the total number of particles is $N_X \times N_Y \times N_Z$. $V=V_H(x)=\frac{1}{2}x^2$ and $k=k_H$ for the harmonic lattice; $V=V_{FPU}(x)=\frac{1}{2}x^2+\frac{1}{4}x^4$ and $k=k_{FPU}$ for the FPU lattice. We use weak harmonic springs to connect the two parts. The Hamiltonian for the connecting springs, H_{int}, is

$$H_{int} = \sum_{m=1}^{N_Y}\sum_{n=1}^{N_Z} k_{int}V_H(|\vec{r}_{N_{FK},m,n;N_{FK}+1,m,n}| - a).$$ (3)

We put two Nośe-Hover[11] heat baths with different temperatures T_L and T_R to the left end and right end of the system so as to establish heat flux along the X direction. That is, the particles for $l=1$ and N_x, $m=1,2,3,\ldots,N_Y, n=1,2,3,\ldots,N_Z$ are coupled with Nośe-Hover heat baths at temperatures T_L and T_R, respectively. Initially, all particles are in the equilibrium position. A fixed boundary condition is used along the X direction (temperature gradient direction). A periodic boundary condition is applied in the Y direction, while there is a free boundary condition in the Z direction. Initially, $\vec{q}_{0,m,n}=(0,ma,na), \vec{q}_{N_X+1,m,n}=((N_X+1)a,ma,na)$, $\vec{q}_{l,1,n}=\vec{q}_{l,N_Y+1,n}-N_Ya\hat{y}, \vec{q}_{l,m,1}=(la,ma,a)$, and $\vec{q}_{l,m,N_Z}=(la,ma,N_Za)$.

The substrate, represented by the potential V_s, is added to the 3D arrays of harmonic oscillators. We call this the 3D FK model, which has the Hamiltonian $H_{FK}=H_H+V_s$. The right segment is the 3D FPU lattice with the Hamiltonian H_{FPU} that is given in Eq. (2). The equations of motion (EOMs) of all particles are $\dot{\vec{p}}_{l,m,n}=\vec{f}_s-\partial H/\partial\vec{q}_{l,m,n}$ for $l=2,\ldots,N_X-1$, and $\dot{\vec{p}}_{l,m,n}=\vec{f}_s-\partial H/\partial\vec{q}_{l,m,n}-\xi_{l,m,n}\vec{p}_{l,m,n}$ for $l=1$ and N_X where $\vec{f}_s$ is the force from the substrate, and the auxiliary variables $\xi_{l,m,n}$ are described by the equations[11] $\dot{\xi}_{l,m,n}=1/\mathcal{Q}(\vec{p}_{l,m,n}^2/3k_BT-1)$. T is the temperature of the Nośe-Hover heat bath on the left end (T_L) or the right end (T_R) and $\mathcal{Q}$ is the coupling parameter between the thermal bath and the system. We set the same value $\mathcal{Q}=1$ as in the 1D and 2D cases.

In our simulation, we set $z_{eq}=a$, which means that the equilibrium distance between substrate and lattice equals the lattice constant. In the Lennard-Jones potential the cutoff distance is about twice the of equilibrium distance, $2z_{eq}$. This indicates that the effect from the substrate is neglected when $z>2z_{eq}$.

The local temperature is defined as

$$\frac{3}{2}k_BT_{l,m,n} = \frac{1}{2}m\langle\vec{v}_{l,m,n}^2\rangle,$$ (4)

where k_B is the Boltzmann constant. The local heat flux $J_{l,m,n}$ along the temperature gradient is defined as the energy transfer per unit time from the particle labeled (l,m,n) to the nearest particle $(l+1,m,n)$ along the X direction:

$$J_{l,m,n} = -\vec{v}_{l+1,m,n} \cdot \vec{F}_{l+1,m,n;l,m,n}$$
$$= -k\vec{v}_{l+1,m,n} \cdot \frac{\partial V(|\vec{r}_{l+1,m,n;l,m,n}| - a)}{\partial|\vec{r}_{l+1,m,n;l,m,n}|}\frac{\vec{r}_{l+1,m,n;l,m,n}}{|\vec{r}_{l+1,m,n;l,m,n}|},$$ (5)

where $k=k_H, k_{FPU}$, or k_{int}, depending on the site along the X direction. In our study, we are concerned only with the heat flux flowing along the X direction. Then we can denote the flux from the particles in the lth section to the next section in the X direction as $J_l=\sum_{m=1}^{N_Y}\sum_{n=1}^{N_Z}J_{l,m,n}$. The total flux of the system can be written as follows:

$$J = \left\langle\frac{1}{N_X}\sum_{l=1}^{N_X}J_l\right\rangle.$$ (6)

We use J_+ to denote the heat current when the high-temperature bath is attached to the FK part and the low-temperature bath is attached to the FPU part; J_- is the heat flow when the heat baths at the two ends are swapped.

III. ANALYSIS OF VIBRATIONAL SPECTRA

After some numerical studies, we found that, under the same parameter settings as in the 1D and 2D cases, rectification still exists in our 3D model, but it is very small compared with the 1D and 2D cases. The rectification is of the order of 10. In order to make our model more efficient, we need to optimize the parameters. We should point out that searching for suitable parameters as in the 1D case to obtain

optimum thermal rectification is not wise since we have too many parameters. On the other hand, we already know that the rectification is determined by interface properties, such as vibrational spectra and interface thermal resistance. Therefore, we decided to do some analytical analysis of the spectra in both segments.

A. Vibrational spectra of the 3D FK lattice

At low temperature, we can linearize the FK model around the equilibrium position $\vec{q}^{\,0}_{l,m,n}=(x^0_{l,m,n}=x^0_l=la, y^0_{l,m,n} =y^0_m=ma, z^0_{l,m,n}=z^0_n=na)$. In this case, all first-order partial derivatives vanish, namely, $(\partial/\partial r)V_s(x_l,y_m,z_n)|_{\vec{q}_{l,m,n}=\vec{q}^{\,0}_{l,m,n}}=0$, where r is x_l, y_m, and z_n, so all crossed terms are also zero. The nonzero terms are $(\partial^2/\partial x^2_l)V_s(x_l,y_m,z_n)|_{\vec{q}_{l,m,n}=\vec{q}^{\,0}_{l,m,n}} =C^1_n$, $(\partial^2/\partial y^2_m)V_s(x_l,y_m,z_n)|_{\vec{q}_{l,m,n}=\vec{q}^{\,0}_{l,m,n}}=C^2_n$, and $(\partial^2/\partial z^2_n) \times V_s(x_l,y_m,z_n)|_{\vec{q}_{l,m,n}=\vec{q}^{\,0}_{l,m,n}}=C^3_n$, where $C^1_n=C^2_n=A_0(z_{eq}/z^0_n)^6$, and $C^3_n=[12A_0/(2\pi)^2][13(z_{eq}/z^0_n)^{14}-7(z_{eq}/z^0_n)^8]$.

Therefore, H_{FK} can be divided as three separated components, namely, $H_{FK}=H_{xx}+H_{yy}+H_{zz}$; each component is related only with the freedom in its corresponding direction. We thus can obtain the EOMs of the particle (l,m,n) in three components. For example, the EOM for the x component is $d^2\delta x_l/dt^2=-\partial H_{xx}/\partial \delta x_l=k(\delta x_{l+1}+\delta x_{l-1}-2\delta x_l)-C^1_n\delta x_l$. The EOMs for the y and z components are in the same form but replacing x by y or z and C^1_n by C^2_n or C^3_n, respectively.

We now look for solutions of the plane wave $e^{-iKa-i\tilde{\omega}t}$. K is the wave vector and $\tilde{\omega}$ is the frequency. From $d^2q/dt^2 =-\tilde{\omega}^2q$ we can obtain the dispersion relations in the X, Y, and Z directions directly if we consider periodic boundary conditions along each direction,

$$\tilde{\omega}^2_i(K) = \sum_{n=1}^{N_z}[2k + C^i_n - 2k\cos(Ka)] \quad (i = 1,2,3). \quad (7)$$

The primitive translation vectors of our simple cubic lattice are taken as the following set: $a_1=a\hat{x}$, $a_2=a\hat{y}$, $a_3=a\hat{z}$. Here $\hat{x},\hat{y},\hat{z}$ are orthogonal vectors of unit length. The reciprocal lattice of our simple cubic lattice is itself a simple cubic lattice with lattice constant $2\pi/a$. The primitive translation vectors of the reciprocal simple cubic lattice are $b_1 =(2\pi/a)\hat{x}$, $b_2=(2\pi/a)\hat{y}$, and $b_3=(2\pi/a)\hat{z}$. Therefore, $i =1,2,3$ corresponds to the [100], [010], and [001] directions, respectively. Equation (7) gives the dispersion relations of the polarization in the X, Y, and Z directions.

C^i_n are the gaps of all branches at zero wave number induced by the substrate. The phonon band of the 3D FK model is $\sqrt{C^i_n}<\tilde{\omega}^i_n<\sqrt{4k_{FK}+C^i_n}$, $n=1,\dots,N_z$, $i=1,2,3$. $C^i_n \propto (1/z^0_n)^\delta$, $z^0_n=na$, and $\delta=6$ for $i=1,2$ and $\delta=8$ for $i=3$; therefore C^i_n decreases to zero asymptotically very fast.

In Fig. 1, we show the dispersion relationship. We can see that the frequency has two main branches. One branch is located in the high-frequency region $\sqrt{C^i_n}<\tilde{\omega}^i_n<\sqrt{4k_{FK}+C^i_n}$ $(n=1, i=1,2,3)$, and is induced by the strongest effect of the substrate on the contact layer. Another branch is located in the low-frequency region and is induced by the effect of the substrate on the inner layers, $\sqrt{C^i_n}<\tilde{\omega}^i_n<\sqrt{4k_{FK}+C^i_n}$ $(n>1, i=1,2,3)$. The low-frequency regions almost overlap with
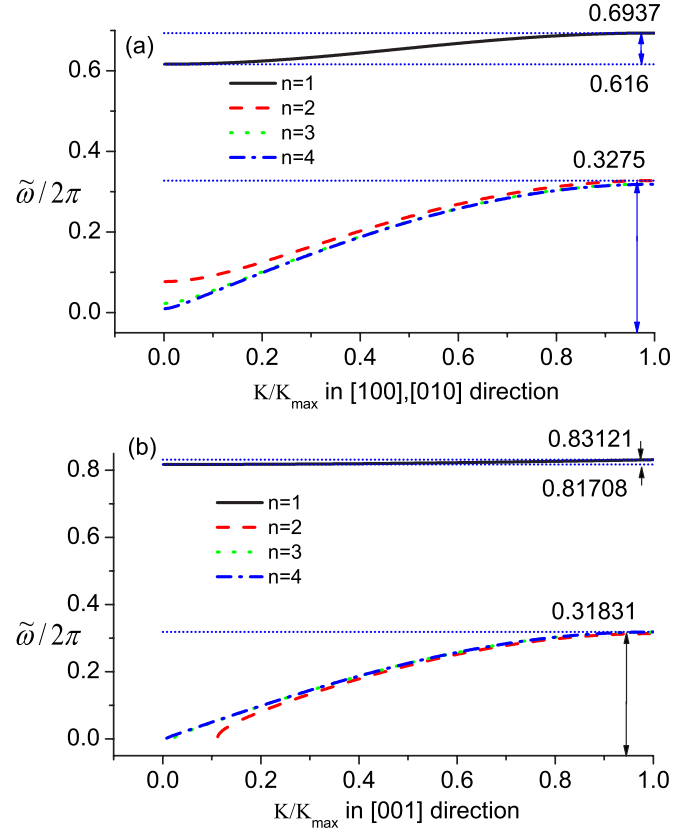

FIG. 1. (Color online) Dispersion relationship of the 3D FK model according to Eq. (7). $A_0=15$, $K_{FK}=1$. (a) Dispersion relationship for the polarization in the X,Y directions. (b) Dispersion relationship for the polarization in the Z direction. Horizontal lines are guidelines for the boundary of different regions and numbers are the corresponding values of the lines along the vertical axis. In both (a) and (b) the curves for $n=3$ and 4 are almost indistinguishable.

the vibrational spectra of harmonic oscillators,[12] $0<\tilde{\omega}^i_n <\sqrt{4k_{FK}}$ $(i=1,2,3)$. The dispersion relation for the 3D FK model in Eq. (7) has a similar form as in the 1D Morse model[5] or the 1D FK model.[6,7] The difference between the 3D and 1D FK models is the additional low-frequency branch induced by the inner layers. We will show later that in the low-temperature limit, vibrations of the 3D FK model concentrate in the high-frequency branch as in low-dimensional cases, while in the high-temperature limit vibrations concentrate in the low-frequency branch. This is because in the high-temperature limit the kinetic energy is much larger than the substrate energy. In this case particles have large enough kinetic energy to jump out of the valleys of the substrate potential and vibrate almost like harmonic oscillators with low frequency, while in the low-temperature limit, the substrate energy is much larger than the kinetic energy. In this case, particles are confined in the valleys of the substrate and oscillate with high frequency.

For a specific parameter setting, such as $A_0=15$, $k_{FK}=1$, we have $\tilde{\omega}/2\pi \in [0,0.327]\cup[0.616,0.694]$ in the [100] and [010] directions and $\tilde{\omega}/2\pi \in [0,0.318]\cup[0.817,0.831]$ in the [001] direction according to Eq. (7). This is shown in Fig. 1. We should point out that there is a slight difference of vibration frequency between a system with finite size and
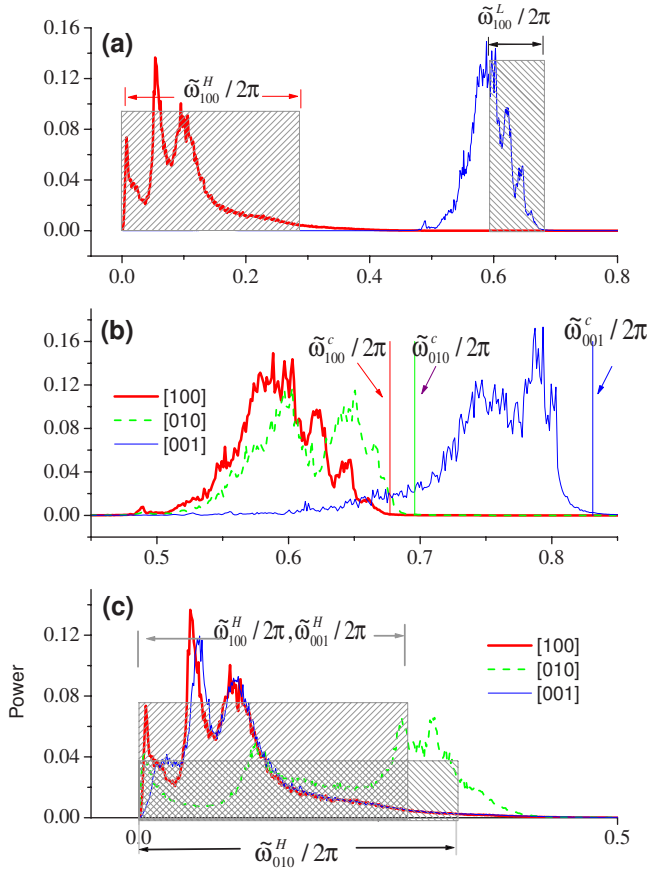
FIG. 2. (Color online) Vibrational spectra of the 3D FK model and the comparison between analytical results and numerical ones. Curves are from DFFT. Analytical ones are given by the hatched boxes. (a) Curves are the vibration bands obtained by DFFT of velocity in [100] direction at low (right curve) and high temperature limits (left curve). (b) Vibrational band from each direction at low-temperature limit. (c) Vibration band from each direction at high-temperature limit. The vertical lines in (b) are the upper bounds of the theoretical prediction.

one with infinite size. For a specific structure with $N_x = 12$, $N_y = 6$, $N_z = 6$, a periodic boundary condition along the Y direction and free boundary conditions along the X and Z directions, we obtain that $\tilde{\omega}/2\pi \in [0, 0.286] \cup [0.599, 0.677]$ in the [100] direction, $\tilde{\omega}/2\pi \in [0, 0.329] \cup [0.618, 0.696]$ in the [010] direction, and $\tilde{\omega}/2\pi \in [0, 0.273] \cup [0.835, 0.835]$ in the [001] direction by solving the EOMs.

If we do a discrete fast Fourier transformation[13,14] (DFFT) of the velocity in each direction directly, we can get the vibration band or energy density of the vibration frequency in each direction. A comparison of the analytic result and the numerical vibrational band by the DFFT are shown in Fig. 2. We compare the analytic and numerical bands in one direction at two limits in Fig. 2(a). The bands in three directions at a relatively low temperature are shown in Fig. 2(b) and at the high-temperature limit in Fig. 2(c). The superscript H or L of ω represents the vibrational band in the high- and low-temperature limits, respectively. The superscript c of $\tilde{\omega}$ in Fig. 2(b) represents the cutoff frequency predicted by the analytic approach. The subscript on ω means the direction of

the corresponding wave vector for the vibrational band. From Fig. 2, we can see that our analytic predictions for the two limits (relative high and low-temperature limits) cover the numerical vibrational bands very well.

B. Vibrational spectra of the 3D FPU lattice

In this section we study the bands in a 3D FPU lattice. To be self-consistent we start from the 1D FPU. Recently, Li *et al.*[15] introduced an effective phonon theory for general 1D nonlinear lattices, from which one can obtain the effective phonon frequency

$$\tilde{\omega}^2 = \alpha(\omega^2 + \gamma). \tag{8}$$

For the FPU model, we have

$$\alpha = \frac{\left\langle \sum_{i=1}^{N} (\delta x_{i,i+1})^2 \right\rangle + \left\langle \sum_{i=1}^{N} (\delta x_{i,i+1})^4 \right\rangle}{\left\langle \sum_{i=1}^{N} (\delta x_{i,i+1})^2 \right\rangle}$$

$$= 1 + \frac{\int_{-\infty}^{\infty} \phi^4 e^{-V/T} d\phi}{\int_{-\infty}^{\infty} \phi^2 e^{-V/T} d\phi}. \tag{9}$$

$\gamma = 0$ for a system without on-site potential, $\omega = 2\sqrt{k} \sin(K\pi/N)$ is the spectrum of a chain of harmonic oscillators, and T is the system temperature. For the FPU model, $V = k_{FPU}(x^2/2 + x^4/4)$. In the high-temperature limit, the quartic term is dominant; we can thus obtain an approximate expression for α,

$$\alpha \approx 1 + \frac{\Gamma(1/4)}{2\Gamma(3/4)} \sqrt{\frac{T}{k_{FPU}}} \approx 1 + \frac{3}{2} \sqrt{\frac{T}{k_{FPU}}}. \tag{10}$$

Here we have used $\Gamma(1/4)/\Gamma(3/4) = 2.958 \approx 3$. Thus the effective phonon bands of the 1D FPU model can be written as

$$\tilde{\omega}^2 = \alpha \omega^2 \cong 4k_{FPU} \left(1 + \frac{3}{2} \sqrt{\frac{T}{k_{FPU}}}\right) \sin^2(K\pi/N). \tag{11}$$

Therefore, the effective phonon band of the FPU model under different temperatures and interaction constants is

$$0 < \tilde{\omega}_{FPU} < \sqrt{4k_{FPU} + 6\sqrt{Tk_{FPU}}}. \tag{12}$$

This formula gives very good agreement with the numerical results at arbitrary interaction constant and temperature in our investigation, $0 < k_{FPU} < 1$, $0 < T < 0.5$ as shown in Fig. 3.

If we calculate the band directly from Eq. (12), we obtain that $\tilde{\omega}_{FPU}^L \in [0, 1.03]$ at $T = 0.01$ and $\tilde{\omega}_{FPU}^H \in [0, 1.35]$ at $T = 0.15$. For comparison, we also draw the theoretical prediction given in our previous work,[7] in which the vibrational band for the FPU model in the low-temperature limit is $\tilde{\omega}_{FPU}^L \in [0, 0.89]$ and compare with the numerical result at
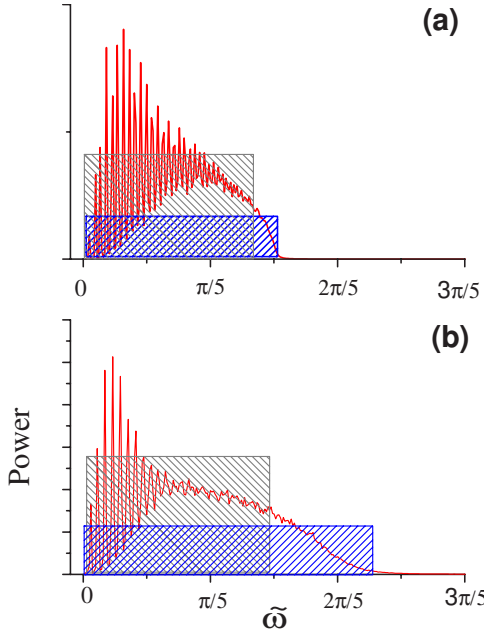
FIG. 3. (Color online) Spectra of 1D FPU model at low (a) and high (b) temperature. Higher hatched boxes are spectra of the 1D FPU model given in Ref. 7. Lower hatched boxes are spectra given by Eq. (12) and curves are numerical results by DFFT. $k_{FPU}=0.2$. $T=$(a) 0.01 and (b) 0.15. The agreement between the analytical and numerical results is very good.

$T=0.01$, while in the high-temperature limit $\widetilde{\omega}_{FPU}^{H}$ $\in[0,0.94]$. A comparison among the two predictions and numerical results is shown in Fig. 3. The lower boxes cover the numerical curves very well. We can see that the prediction by Eq. (12) is much better than the prediction by the previous work.[7]

The analysis of the effective phonon bands is also suitable for the 3D case. The interaction potential in the Hamiltonian of the 3D FPU in Eq. (2) consists of three individual parts and each part has the same form as in the 1D case when we neglect the energy interchange among different directions. We can write the Hamiltonian as $H_{FPU}=H_{100}+H_{010}+H_{001}$. Here H_{100} is $H_{100}=\Sigma_{l=1}^{N_X}\Sigma_{m=1}^{N_Y}\Sigma_{n=1}^{N_Z}[(v_x)_{l,m,n}^2/2+kV(|\vec{r}_{l+1,m,n;l,m,n}|-a)]$; by replacing x by y, and/or z, one can obtain H_{010} and H_{001}, respectively.

Each part contains the kinetic energy along one primitive axis and the interaction potential among particles originally on the corresponding primitive axis. Since $V(r)$ has the same form as $V(x)$ in one dimension, we can infer that the effective phonon band along each primitive axis is the same as in the 1D case.

The phonon bands in the X, Y, and Z directions from numerical results and the theoretical prediction are plotted in Fig. 4. We can see that the theoretical predictions by Eq. (12) agree with the numerical results very well in the 3D case. The slight difference might come from the different boundary conditions.

C. Match and mismatch of bands of the FK and FPU lattices

From the above analysis, we see that the vibrational bands of the 3D FPU lattice always concentrate in the low-
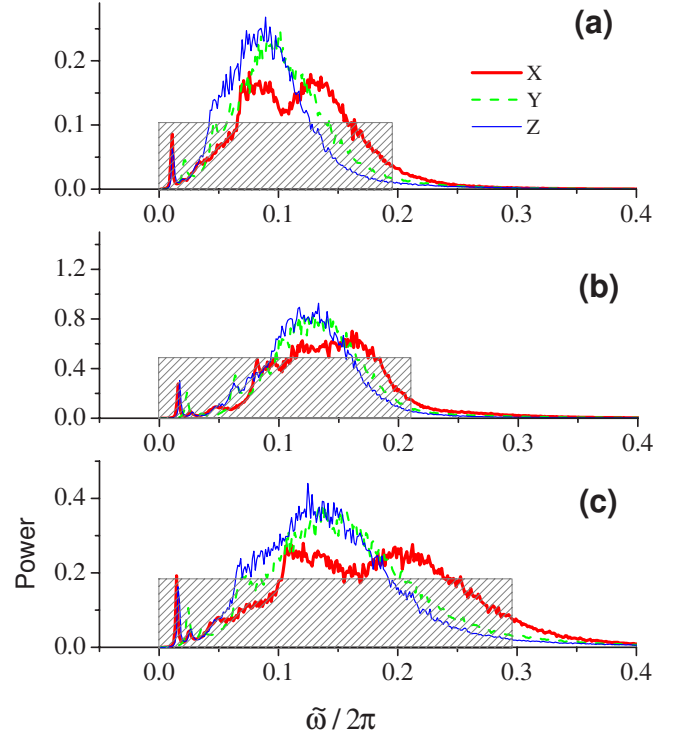

FIG. 4. (Color online) Spectra of 3D FPU model with different parameters. (a) $T=0.04$ and $k_{FPU}=0.2$. (b) $T=0.15$ and $k_{FPU}=0.2$. (c) $T=0.1$ and $k_{FPU}=0.5$. Boxes are spectra of the 3D FPU model given by theoretical prediction in Eq. (11) and curves are numerical results by DFFT.

frequency region as in low-dimensional cases. In contrast, the 3D FK lattice has two main branches, which correspond to low- and high-temperature limits, respectively, and the two regions separate from each other when the parameters are chosen appropriately. Therefore, by choosing suitable parameters, it is possible to match and mismatch the bands of the two parts when swapping the temperature at the two ends, thus leading to good thermal rectification. In this section, we show how to select suitable parameters of the system and suitable temperatures on the system to obtain the best rectification.

In Fig. 5, we show how the bands of the FK and FPU lattices change with the system parameters. In Figs. 5(b) and 5(c), we can see that the width and position of the vibrational band of the FK part change with the barrier height of the substrate potential and system temperature. In Fig. 5(b), the spectra broaden from the low- to the high-frequency region when the barrier height increases. However, in Fig. 5(c), the spectral shift from the high- to the low-frequency region when the temperature is increased. The physical mechanism here is clear. When A_0 is small, the particles have large enough kinetic energies to jump out of the potential valleys. The substrate potential becomes negligible. The FK lattice degenerates to a harmonic one. When we increase the barrier height A_0, the substrate becomes dominant and the particles are confined in the valley of the substrate potential. Thus the atoms oscillate at very high frequency. In Fig. 5(c), we fix the barrier height and change temperature. At low temperature the substrate is dominant; thus the particles are confined
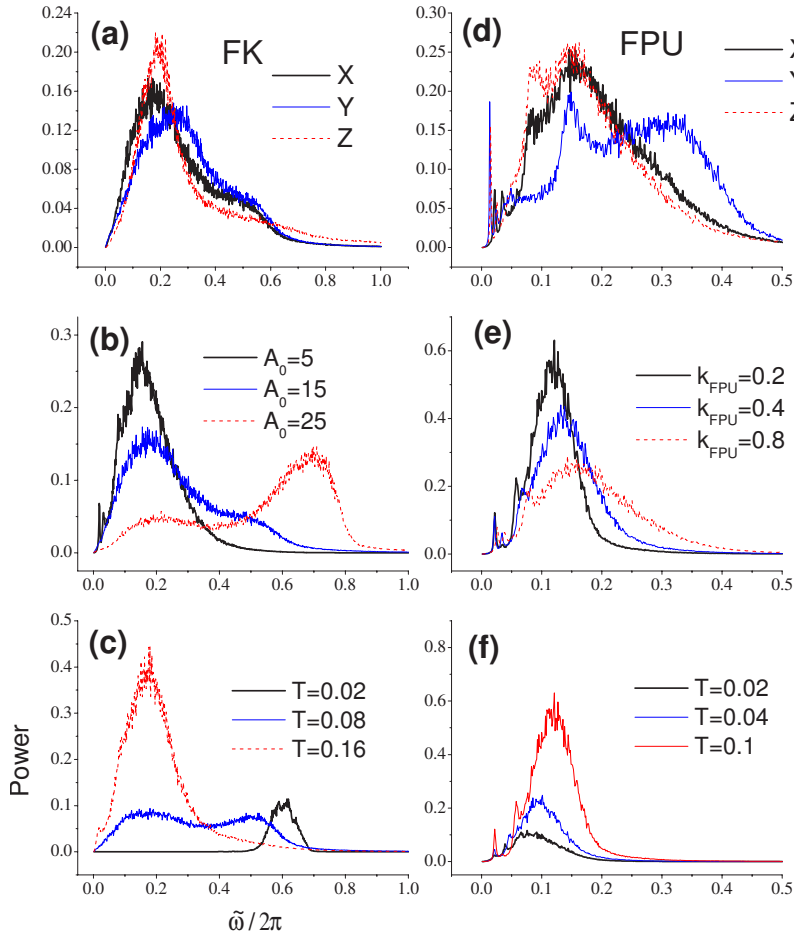
FIG. 5. (Color online) (a),(b),(c) Vibration spectra of the 3D FK lattice under different conditions. (d),(e),(f) Spectra of the 3D FPU lattice under different conditions. (a) and (d) are vibration spectra in the X, Y, Z directions with $T=0.1$, $A_0=15$, $K_{FPU}=1$. (b) and (e) are vibration spectra along the X direction with different parameters such as A_0, K_{FPU}, with fixed temperature $T=0.1$. (c) and (f) are vibration spectra along the X direction at different temperatures with fixed parameters $A_0=15$, $K_{FPU}=0.2$.

in the valley of the substrate. When we increase the temperature, the kinetic energy of the particles becomes larger and larger. It eventually becomes dominant compared with the effect from the substrate. So, when the temperature is increased, the main part of the spectrum shifts from high frequency (substrate is dominant) to low frequency (kinetic energy is dominant).

In Figs. 5(d)–5(f), we show the spectra of the FPU lattice. In Fig. 5(d), the slight difference among the bands from each direction should come from the different boundary conditions in each direction, as we analyzed previously. In Figs. 5(e) and 5(f), we show how the bands change with temperature and interaction constant. We can see that the band becomes broader and broader as the temperature and interaction constant are increased. This result is consistent with our theoretical analysis.

From the above analysis, we can write the effective phonon band of the FK part in one formula as $\sqrt{C} < \tilde{\omega}^i < \sqrt{4k_{FK}+C}$, where $C=C_n^i$ ($n>1$) in the high-temperature limit and $C=C_1^i$ (a finite value only related to barrier height) in the low-temperature limit. C_n^i decreases to zero asymptotically very fast. For example, $C_3^i \approx 0.001\,37C_1^i$ and $C_2^i \approx 0.0156C_1^i$. From these two limits, we can see that C is temperature dependent. We will show that it decreases with increasing temperature. This is consistent with previous studies[5] of the 1D model.

Figures 5(b) and 5(c) tell us that the gap C depends on temperature and barrier height. Therefore, we may write it as

$C(T,A_0)$. The upper limit of $C(T,A_0)$ is determined by A_0 through Eq. (7), and $C(T,A_0)$ decreases monotonically to zero with increasing temperature. Following a similar concept introduced in Ref. 16, we define a quantity η to describe the nonlinearity due to the substrate,

$$\eta = \frac{\varepsilon_s}{\varepsilon_s + T},$$

$$\mathfrak{C}(T) = \eta C_{up}(A_0), \qquad (13)$$

where $\varepsilon_s = \langle V_s \rangle$ is the temporal average of the substrate potential, which has different values at different temperatures, and $C_{up}(A_0)$ is the upper limit of the gap. In this way, the quantity $\mathfrak{C}(T)$ has the same behavior as the gap $C(T,A_0)$ as temperature changes, and they have the exact same values in the two limits (high- and low-temperature limits). The behavior of η with temperature is shown in Fig. 6. It decreases from a finite value to 0 asymptotically as temperature increases. Thus we may use $\mathfrak{C}(T)$ to approximate the gap $C(T,A_0)$. We can then obtain the effective phonon band of the FK model under different temperatures and parameters,

$$\sqrt{\mathfrak{C}(T)} < \tilde{\omega}_{FK} < \sqrt{4k_{FK} + \mathfrak{C}(T)}, \qquad (14)$$

where $\mathfrak{C}(T)$ is determined by Eq. (13). In Fig. 7, we show the spectra from Eq. (14) at two limits and the numerical one obtained by DFFT.
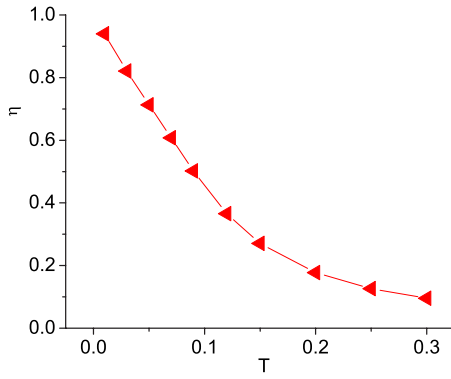
FIG. 6. (Color online) Nonlinearity parameter η [refer to Eq. (13) for definition] versus temperature.

For the FK lattice, the spectra at the low- and high-temperature limits separate from each other, while in the FPU lattice, the spectrum always concentrates at low frequency. So when the left part is at high temperature and the right part is at low temperature, the vibrational bands of the two parts are matched with each other as shown in Fig. 8(a). When swapping the temperatures of the two parts, the bands of the two parts are mismatched with each other as shown in Fig. 8(b). In terms of the match or mismatch of the bands when changing temperature under suitable parameters, the system should have strong rectification since matched bands indicates a large heat flux along the system and mismatched bands inhibits heat flux along it. In the following part, we will give numerical evidence to support the above analysis.
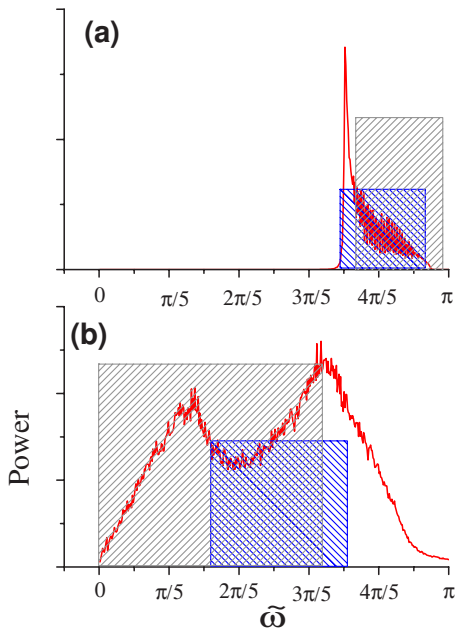

FIG. 7. (Color online) Spectra of 1D FK model at different temperatures. $T=$ (a) 0.01 and (b) 0.15. High hatched boxes are spectra given in Ref. 7 at the low- and high-temperature limits. Lower hatched boxes are spectra given by Eq. (13) and curves are numerical results by DFFT.
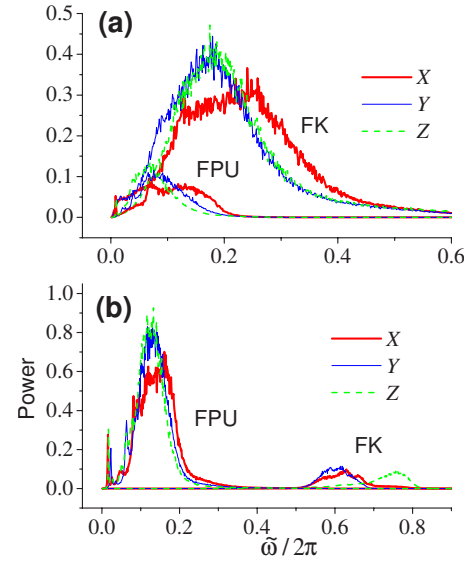

FIG. 8. (Color online) Matched (a) and mismatched (b) vibration spectra in the X, Y, Z directions of the two parts with different parameters $A_0=15$, $K_{FPU}=0.2$. (a) $T_L=0.15$, $T_R=0.02$, and (b) $T_L=0.02$, $T_R=0.15$. In (a) the upper three curves are for the FK model, the lower three curves are for the FPU. In (b), the left three curves are for the FPU and the right three curves are for the FK model. Thick (red), thin (blue), and dashed (green) curves are for X, Y, and Z directions, respectively.

IV. THERMAL RECTIFICATION IN THE 3D FK-FPU MODEL

After theoretical analysis of the vibrational spectra, we select $A_0=15$, $k_{FK}=1$, and $k_{FPU}=0.2$. We denote the temperature as $T_L=T_0(1-\Delta)$, $T_R=T_0(1+\Delta)$. So T_0 is the system average temperature and Δ is the normalized temperature difference.

In Fig. 9, we show the heat flux and rectification versus Δ. The ratio of heat fluxes, $|J_+/J_-|$, the rectification, can be as much as several thousands. Some properties observed in 1D and 2D are still observable in 3D case. The exponential dependence of the rectification on the normal temperature is also true. For negative Δ, we clearly see the decrease of $|J_-|$ as $|\Delta|$ increases. This interesting phenomenon, so-called negative differential thermal resistance, is a typical phenomenon in nonlinear lattices. It is very essential for the design of thermal transistor.[17] Therefore, one also expects that the 1D thermal transistor model can be extended to higher dimensions.

The exponential dependence of rectification on Δ obeys the following formula:

$$|J_+/J_-| \propto \exp(c\Delta), \qquad (15)$$

where $c=4.342$ is different from the coefficient found in the 2D case.[9]

In Fig. 10, we show how the rectification changes with the system temperature. As in the low-dimensional case, there exists an optimum temperature under which the system has the largest rectification. Away from the optimum temperature, the rectification decreases. But the effective temperature
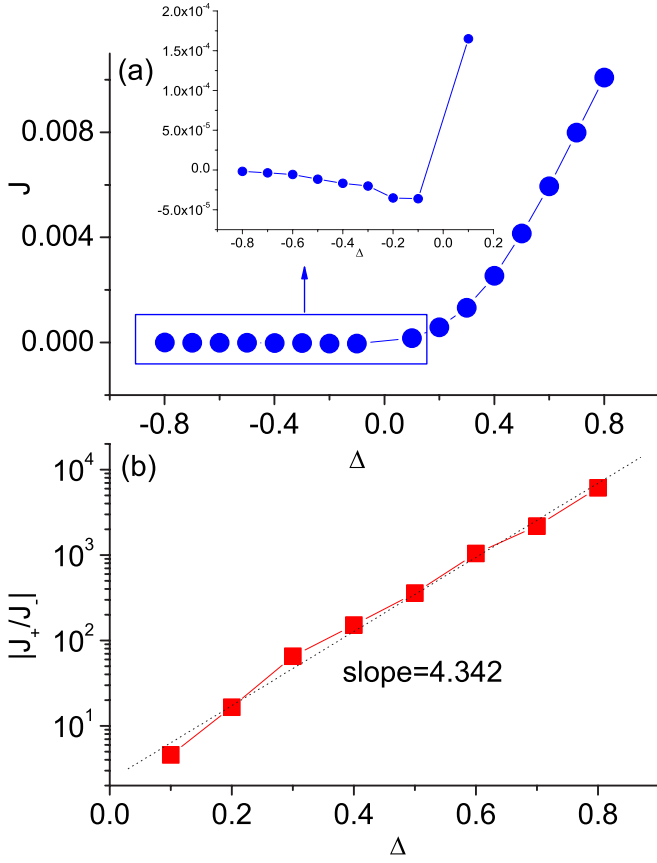
FIG. 9. (Color online) (a) Heat current J versus the dimensionless temperature difference $\triangle$ at temperature $T_0 = 0.06$. (b) Rectification $|J_+/J_-|$ versus dimensionless temperature difference. The dotted line has a slope of 4.342. In our numerical simulation, $N_X = 12$, $N_Y = 6$, and $N_Z = 3$.

FIG. 10. (Color online) (a) Rectification versus temperature T_0 when fixed $\Delta = 0.5$. (b) Rectification versus system temperature T_0 by fixing the temperature difference $T_L - T_R = 0.06$. $T_0 = (T_L + T_R)/2$, $\Delta = (T_L - T_R)/(2T_0)$. In our numerical simulation, $N_X = 12$, $N_Y = 6$, and $N_Z = 3$.

V. CONCLUSIONS AND DISCUSSION

In this paper, we have proposed an efficient 3D thermal rectifier consisting of two parts; one part consists of layered

region is very broad. W_T is the quantity defined as the width of the effective temperature range T_e over half the value of the largest rectifying efficiency. It is about 0.04 in this case.

In Fig. 10(b), we keep the absolute temperature difference as a constant $|T_L - T_R| = 0.06$ and change the system temperature $T_0 = (T_L + T_R)/2$. From this figure, we can see that, with this kind of temperature difference, the system works very well at low temperature.

Finally, in Fig. 11 we show the dependence of rectification on the system size. We change the number of particles along the direction perpendicular to the temperature gradient, the Y direction, and the Z direction (perpendicular to the contact plane with the substrate). In this figure, the rectification decreases slowly as the system size increases. From the phonon band theory and the relationship between the rectification and the convolution of bands from the two parts, which was obtained in our previous work,[7,9] the decreasing trend should stop at a certain system size since the increase of the system size along the direction perpendicular to temperature gradient will not change the temperature jump at the interface. The vibrational bands of the two parts will tend to the theoretical prediction as the system size increases. We should point out that the oscillation of the rectification in our results is due to the fluctuation of J_-, because its amplitude is too small.
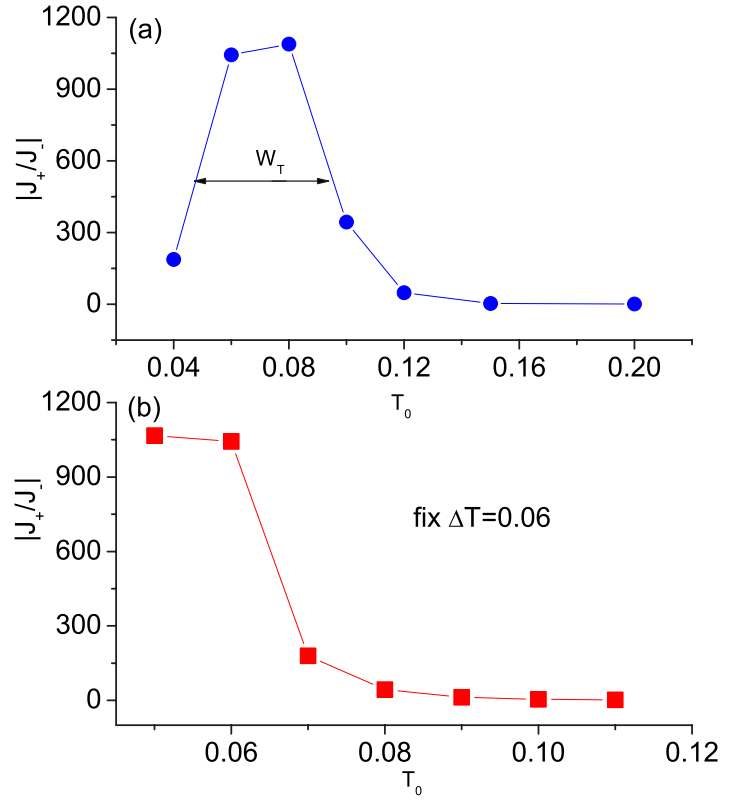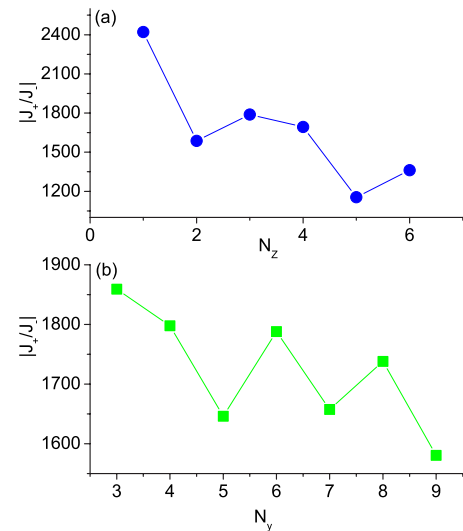

FIG. 11. (Color online) (a) Thermal rectification versus the number of particles along the Z direction. $N_X = 12$, $N_Y = 6$. (b) Thermal rectification versus the number of particles along the Y direction. $N_X = 12$, $N_Z = 3$.

harmonic oscillators coupled with the substrate, namely, a 3D FK lattice, and the other part is the 3D FPU lattice. First of all, we have studied analytically and numerically the vibrational spectra for both the 3D FK and 3D FPU models. For the FK model, the band is concentrated in the high-frequency region, which is mainly induced by the substrate in the low-temperature limit, and shifts to the low-frequency region on increasing temperature; while for the FPU model, the band broadens from a harmonic band slowly as the temperature increases. The different temperature dependence of the bands makes the transition from matched to mismatched bands possible when swapping the temperature at the two ends, and consequently makes it possible to realize thermal rectification.

In fact, the FPU part can be replaced by a 3D harmonic lattice. As in the 1D case, the replacement with the 3D harmonic lattice gives slightly better performance. The reason we chose the FPU lattice is that it is closer to real materials, because the FPU is the simplest model to include the phonon-phonon interaction, which is essential to establish a temperature gradient. As we all know that the phonons in a harmonic lattice of any dimension have no interaction, the heat conductivity is infinite for any harmonic lattice.

The FPU model can be regarded as an approximation of the molecular interaction at equilibrium of an ideal crystal, while the FK model describes a crystal coupled with a substrate. Our study on thermal rectification in these two lattices has general meaning, since the two anharmonic lattices are two representative ones widely studied in different fields of physics (see Refs. 6 and 7, and references therein). Most physical systems can be divided into our two representative models: one with and one without an on-site potential.

Finally, we would like to discuss a possible experiment on the thermal rectifier. Recently, Chang *et al.* have realized a solid state thermal rectifier by using carbon nanotubes (CNTs) and boron nitride nanotubes (BNNTs).[18] The experiment is basically a two-segment device as we proposed.[6,7] They introduced asymmetry by depositing $C_9H_{16}Pt$ on half of a multiwalled nanotube with nonuniform mass loading. Previous studies have demonstrated that the thermal conductivity of 1D CNTs and BNNTs is dominated by phonons.[19,20] So the rectification is caused by the mismatch of vibrational spectra. In the experiment, the rectification is less than 10%. This might be understood as from the absence of the on-site potential. As an alternative, we propose a possible realization of our current 3D model. One may put a nanowire or nano-rod on a semiconductor substrate which will induce an on-site substantial, while the other half of the nanowire on rod is suspended in vacuum.[21] This setup may give higher rectification.

*Electronic address: phylibw@nus.edu.sg

[1] A. Williams, Ph.D thesis, Manchester University, 1966.

[2] G. Y. Eastman, Sci. Am. **218**, 38 (1968).

[3] T. R. Thomas and S. D. Probert, Int. J. Heat Mass Transfer **12**, 789 (1970).

[4] P. W. O'Callaghan, S. D. Probert and A. Jones, J. Phys. D **3**, 1352 (1970).

[5] M. Terraneo, M. Peyrard, and G. Casati, Phys. Rev. Lett. **88**, 094302 (2002).

[6] B. Li, L. Wang, and G. Casati, Phys. Rev. Lett. **93**, 184301 (2004).

[7] B. Li, J. Lan, and L. Wang, Phys. Rev. Lett. **95**, 104302 (2005).

[8] B. Hu and L. Yang, Chaos **15**, 015119 (2005).

[9] J. Lan and B. Li, Phys. Rev. B **74**, 214305 (2006).

[10] J. Rodríguez-Laguna and S. N. Santalla, Phys. Rev. B **72**, 125412 (2005).

[11] S. Nośe, J. Chem. Phys. **81**, 511 (1984); W. G. Hoover, Phys. Rev. A **31**, 1695 (1985).

[12] C. Kittel, *Introduction to Solid State Physics*, 7th ed. (John Wiley and Sons, New York, 1996).

[13] H. P. William *et al.*, *Numerical Recipes* (Cambridge University Press, Cambridge, U.K., 1992).

[14] J. Lan, Ph.D thesis, National University of Singapore, 2007.

[15] N.-B Li, P.-Q Tong, and B. Li, Europhys. Lett. **75**, 49 (2006).

[16] N.-B Li and B. Li, Europhys. Lett. **78**, 34001 (2007).

[17] B. Li, L. Wang, and G. Casati, Appl. Phys. Lett. **88**, 143501 (2006).

[18] C. W. Chang, D. Okawa, A. Majumdar, and A. Zettl, Science **314**, 1121 (2006).

[19] C. W. Chang, W. Q. Han, and A. Zettl, J. Vac. Sci. Technol. B **23**, 1883 (2005).

[20] J. Hone, M. Whitney, C. Piskoti, and A. Zettl, Phys. Rev. B **59**, R2514 (1999).

[21] E. Pop, D. Mann, J. Cao, Q. Wang, K. Goodson, and H. Dai, Phys. Rev. Lett. **95**, 155505 (2005).